Supplementary Material to the article "Impact of domain wall conduction on ferroelectric domain reversal kinetics"

1. Mapping of the domain formation energy $W(l_a, l_c, E)$

The domain formation energy $W = W_S + W_E$ consists of the surface and electrostatic contributions. The positive surface contribution $W_S = w_0 S_0 + w_1 S_\perp$ is the same in the absence and presence of domain wall (DW) conduction, while the electrostatic contribution is different. For semi-spheroidal domain shape, all contributions can be analytically expressed by the semi-axes l_a and l_c. All calculations are performed below for the lithium niobate (LN) parameters $P = 70\,\mu\mathrm{C/cm}^2$, $\varepsilon_a = 85$, and $\varepsilon_c = 30$.

In the absence of DW conduction we have [1, 2]

$$W_E = 2PV_D(E_d f - E)\ , \tag{S1}$$

where, as in the main text, $f = f(l_a\sqrt{\varepsilon_c}/l_c\sqrt{\varepsilon_a})$ is the depolarization factor and $E_d = 4\pi P/\varepsilon_c$ is the depolarization field. This relation coincides with the classical one [3] up to notation. Explicit relations for f can be found in[4]. Because of a very large value of the depolarizing field in LN crystals, $E_d \simeq 2.6$ MV/mm, the electrostatic energy W_E remains positive and unrealistically high up to very large values of E unless the factor of f is very small. This is relevant to the limit of strongly elongated domains, $l_c/l_a \gg (\varepsilon_c/\varepsilon_a)^{1/2} \simeq 0.6$.

Figure S1a shows the contour lines $W(l_a, l_c) = const$ for $E = 5$ kV/mm (which is representative for E_c in stoichiometric lithium niobate (SLN)), $w_0 = 3$ erg/cm^2, and $w_1 = 5w_0$. The energy is measured in eV, while l_a and l_c are given in nm. One sees a single saddle point $l_a^* \simeq 0.87$ nm and $l_c^* \simeq 102$ nm corresponding to the critical energy $W_* \simeq 2.72$ eV. This energy corresponds to the thermo-activation factor $\exp(W_*/k_\mathrm{B}T) \sim 10^{-45}$, which makes the nucleation process unrealistic. Increasing the ratio w_1/w_0 gives no positive effect. Analysis of the expression for $W(E, l_a, l_c)$ shows that the critical values l_a^*, l_c^*, and W_* scale approximately as w_0/E, $w_0/E^{3/2}$, and $w_0^3/E^{5/2}$, respectively, when changing E and w_0 [1]. The behavior of $W_*(E)$ contradicts to the exponential law $\exp(-E_n/E)$ for the nucleation probability. Also, it is unlikely that the value of w_0 is significantly smaller than 3 erg/cm^2.

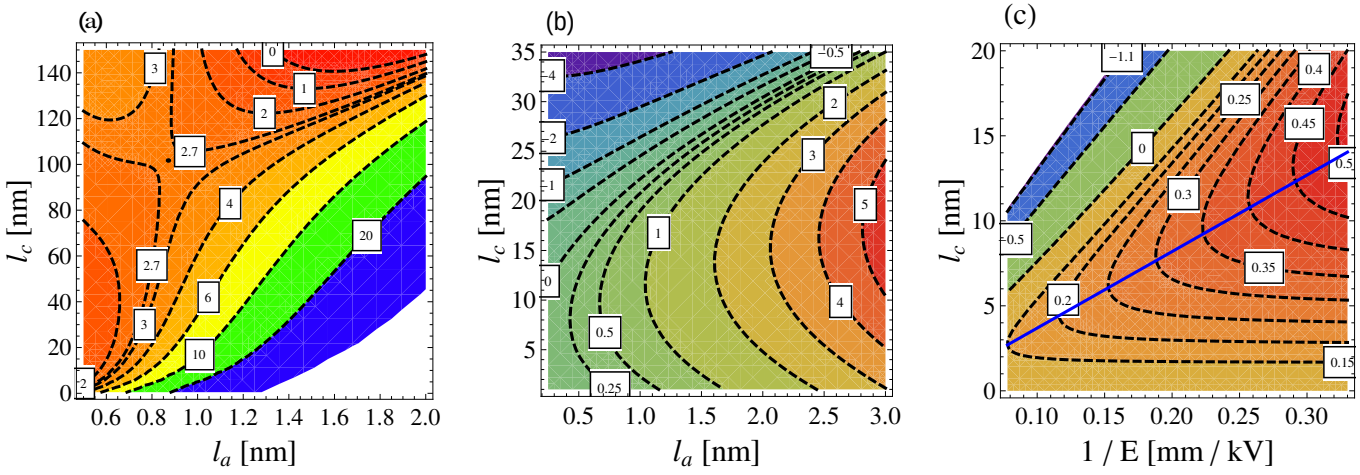

FIG. S1: a) Contour plot $W(l_a, l_c) = const$ for $E = 5$ kV/cm^2, $w_0 = 3$ erg/cm^2, and $w_1 = 5w_0$ in the *absence* of the DW conduction. The saddle point in (a), shown by a dot, corresponds to $W_* \simeq 2.72$ eV, $l_a^* \simeq 0.87$ nm, and $l_c^* \simeq 102$ nm. (b) Contour lines $W(l_a, l_c) = const$ for the same input parameters in the *presence* of DW conduction. (c) Contour lines $W(1/E, l_c) = const$ for the same input parameters and $l_a = l_a^* = 0.5$ nm in the presence of DW conduction. The blue straight line shows the critical value l_c^* versus E corresponding to Eq. (2) of the main text. All values of the domain energy W are given in eV by the insets.

In the presence of DW conduction we have for the electrostatic contribution [1, 2]

$$W_E = -\varepsilon_c E^2 V_D/4\pi f\ . \tag{S2}$$

It is negative and growing $\propto E^2$ in the absolute value. Also, it grows in the absolute value with increasing ratio l_c/l_a facilitating nucleation of elongated domains. The absence of the term PE in Eq. (S2) is caused by the compensation of large bound polarization charges at the DW by free charges.

Figure S1b shows the map of $W(l_a, l_c)$ for the same values of E and $w_{0,1}$. It is essentially different from the map of Fig. S1a: The actual values of W and l_c are relatively low, while the inequality $l_c \gg l_a$ is still holds true. Furthermore,

no true saddle point is present. However, the dependence $W(l_c)$ possesses a maximum at any fixed value of l_a, see Fig. S2a. The smaller l_a, the lower is the point of maximum of $W(l_c)$. These properties indicate that the minimum possible value of l_a and the corresponding maximum value of l_c have to be treated as the critical ones (l_a^* and l_c^*). Dashed lines in Fig. S1c correspond to the contour lines $W(1/E, l_c) = const$ for $l_a = l_a^* = 0.5$ nm and the same values of $w_{0,1}$. The field E ranges here from $\simeq 3$ to 12 kV/mm. The smaller E, the higher is the maximum of $W(l_c)$ and the larger is l_c^*. The straight blue line gives the dependence $l_c^*(E)$; it nicely corresponds to Eq. (1) of the main text. The maps of $W(1/E, l_c)$ with lines $l_c^*(E)$ for, let say, $l_a^* = 0.25$ and 0.75 nm look very similar.

Next, we consider in some detail quantization of the characteristic field E_n, as given by Eq. (2) of the main text. Strictly speaking, the value of $\Lambda = \ln(2l_c^*\sqrt{\varepsilon_a}/l_a^*\sqrt{\varepsilon_c})$ depends on E. However, this dependence is fairly weak in the range $(3-12)$ kV/mm, such that $\Lambda^{1/2} \approx 2$ with a good accuracy. The main uncertainty in the evaluation of E_n comes from the value of the product $w_0 l_a^*$. At $\Lambda = 2$ and room temperature, we have a simple practical relation for E_n:

$$E_n[\text{kV/mm}] \approx 74 \times \left(l_a^*[\text{nm}] \times w_0[\text{erg/cm}^2]\right)^{3/2} . \tag{S3}$$

It shows that the characteristic scale of E_n is 10^2 kV/mm. Also, it enables us to use a single fit parameter E_n instead of two parameters l_a^* and w_0.

Lastly, we consider restrictions on the choice of the surface charge density w_1 relevant to charged sections of DWs. This restriction comes from the value of the exponential factor $\exp(\pi l_a^{*2} w_1/k_B T) = \tau_*/\tau$. This factor can hardly be much larger than 10^8 to deal with reasonable values of τ_*. For $l_a^* = 0.5$ nm, this gives a fairly weak restriction $w_1 \lesssim 10^2$ erg/cm^2, providing, nevertheless, a lot of room for the inequality $w_0 \ll w_1$.

2. The effects of N and E on kinetics of the polarization reversal

The main limiting factor for further increase of N (beyond our maximal value 10^{10}) was the increase of the necessary memory capacity. On the other hand, the values $N = 10^8$ and 10^{10} are sufficient to make the relative temporal fluctuations of the concentrations fairly weak. They are also sufficient to provide representative spatial domain patterns in the considered area – the spatial uniformity in average.

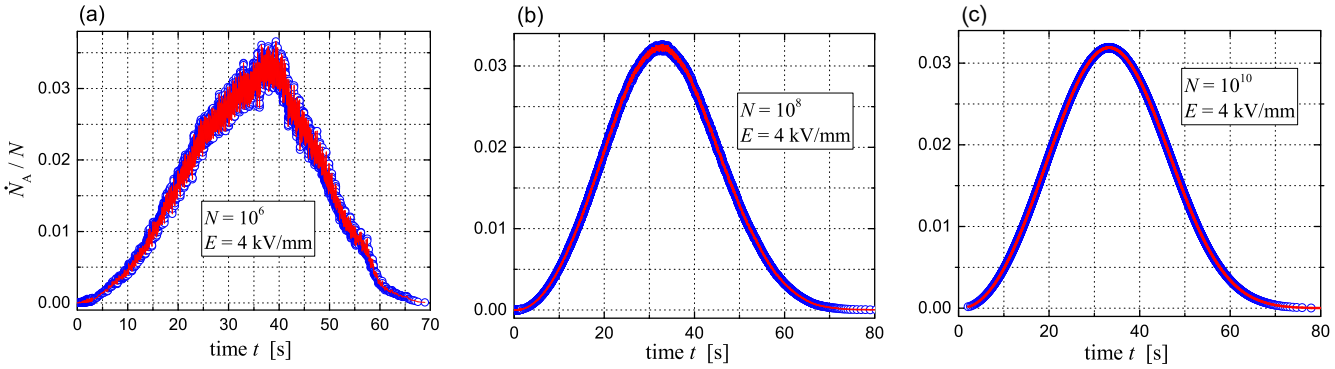

FIG. S2: Dependence $\dot{N}_A(t)/N = dN_A/Ndt$ for $E = 4$ kV/mm and three values of N: Subfigures (a), (b), and (c) correspond to $N = 10^6$, 10^8, and 10^{10}, respectively. In subfigures (b) and (c) the noise is fairly weak, and the points of maxima are almost the same: $t_m \simeq 33.3$ s and $\dot{N}_A(t_m)/N \simeq 0.032$. For $N = 10^6$ the noise is large and accuracy of determination of t_m is insufficient.

Figures S2(a), S2(b), and S2(c) exhibit dependences $\dot{N}_A(t)/N$ (which are more noisy as compared to those of $N_A(t)/N$) for $E = 4$ kV/mm and three values of N, 10^6, 10^8, and 10^{10}. While for $N = 10^6$ the dependence $\dot{N}_A(t)/N$ is clearly noisy, for $N = 10^8$ and 10^{10} is is not noisy and practically the same corresponding to $t_m \simeq 33.3$ s. A similar behavior with increasing N takes place for all values of E in the range $(3-12)$ kV/mm. This is why we considered mostly the case $N = 10^8$.

To show the effect of E on the domain kinetics, we compare the domain patterns generated for $E = 3$ and 4 kV/mm at the same fraction of inverted domains N_A/N. In accordance with Fig. 4a of the main text, this corresponds to substantially different waiting times. Figures S3(a) and S3(b) correspond to $N_A/N \simeq 0.1$ and $t \simeq 300$ and 19 s. Similarly, Figs. S3(c) and S3(d) are generated for $t \simeq 400$ and 25 s, which is relevant to $N_A/N \simeq 0.2$. One can see that the number of domains and their average size in the pairs (a)-(b) and (c)-(d) are strongly different. The average

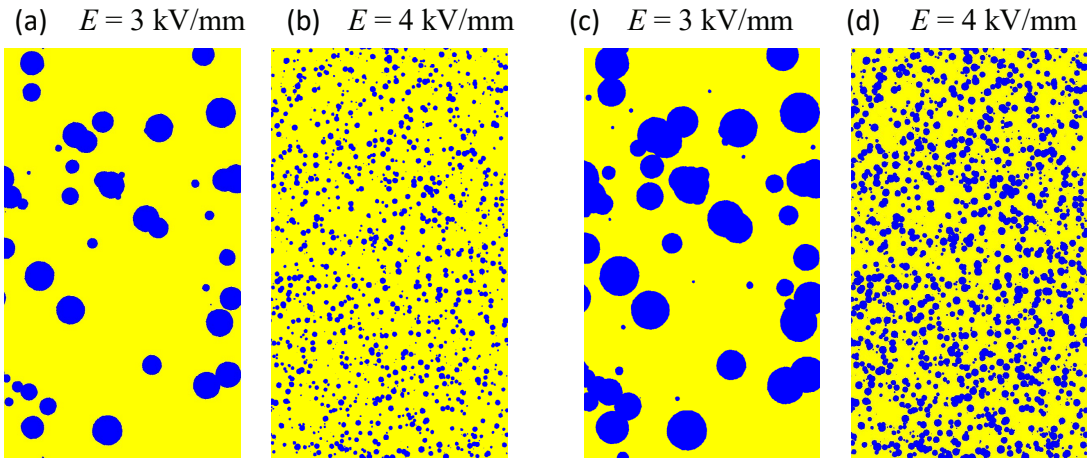

FIG. S3: Comparison of domain patterns for $E = 3$ and 4 kV/mm at approximately the same fractions N_A/N: Patterns (a) and (b) are plotted for $t \simeq 300$ and 19 s, respectively, corresponding to $N_A/N \simeq 0.1$. For patterns (c) and (d) we have $t \simeq 400$ and 25 s leading to $N_A/N \simeq 0.2$.

sizes in (a) and (b) are roughly different by one order of magnitude. Within the whole range $E = (3 - 12)$ kV/mm, this ratio amounts to two orders of magnitude.

It is possible to define the reversal time $\tilde{t}_R$ as the time when the last cell is inverted. With this definition, $\tilde{t}_R$ is about 20% larger than the time $t_R = 2t_m$ used in the main text. Furthermore, the time $\tilde{t}_R$ is subjected to substantially larger fluctuations compared to t_R.

[1] B. Sturman and E. Podivilov, Ferroelectric domain reversal: the role of domain wall conduction, JETP Letters **116**, 246 (2022).
[2] B. Sturman and E. Podivilov, Effect of domain wall conductivity on domain formation energy, Ferroelectrics **601**, 80 (2023).
[3] R. Landauer, Electrostatic considerations in $BaTiO_3$ domain formation during polarization reversal, J. Appl. Phys. **28**, 227 (1957).
[4] L. D. Landau and E. M. Lifshitz, *Electrodynamics of Continuous Media* (Pergamon Press, London, 1960).